International Journal of Solids and Structures 96 (2016) 393–399

Contents lists available at ScienceDirect

International Journal of Solids and Structures

journal homepage: www.elsevier.com/locate/ijsolstr

Parametric investigation of soft-body penetration into parallel-ridged textured surfaces for tactile applications

T.J. Wilde, C.J. Schwartz*

Iowa State University, Department of Mechanical Engineering, 2025 Black Engineering Bldg., Ames, IA 50011, USA

ARTICLE INFO

Article history:
Received 27 January 2016
Revised 31 March 2016
Available online 24 May 2016

Keywords:
Skin tribology
Tactile friction
Surface textures

ABSTRACT

The tribological interactions between skin and textured surfaces has profound impact on both the tactile perception of the product being used, as well as the functionality of the product with regards to friction coefficient. Previous work has shown that parallel-ridged textures have vastly different friction coefficients with regards to the direction of skin sliding, and that penetration of the skin into the voids between ridges not only add contact area but also potential for interlocking. The ability to model skin penetration into textural elements would prove to be very useful for predicting friction; however, the mechanics of the problem are incredibly complex such that they rule out a closed-form analytical solution. The authors investigated soft-body penetration using a non-dimensional computational approach based on the elastic properties of skin, as well as the texture ridge geometry parameters, as well as the normal loading. Model results were verified experimentally. The model was applied to a number of different combinations of ridge parameters and it was found that the amount of penetration could be predicted very well using a simple exponential relationship among the nondimensional terms. Texture groove width and applied normal load played a dominant role in penetration. These results yield a quantitative mechanics model which can be integrated into an overarching frictional model to predict skin on texture behavior due to both adhesion and edge interlocking.

1. Introduction

Tactile friction and perception are of great interest to engineers and product designers because of the number of products which are handled every day that require suitable surface characteristics to serve their function or to please the user. Perception enables us to judge characteristics of materials that we interact with whether they are cosmetic or functional. On the cosmetic side, tactile perception has been shown to influence our perception and feeling toward products (Chen et al., 2009; Childs and Henson, 2007; Barnes et al., 2004). On the other hand, the frictional components of tactile perception can allow us to distinguish between materials (Bergmann Tiest, 2010) and indicate to us if we need to apply more or less force when handling an object whether to influence grip or reduce abrasion. Thus, engineered surfaces are often optimized for their frictional purposes. For example, low friction surfaces such as the mouse pad of a laptop allow for ease of movement while high friction surfaces such as tool handles, phone cases, railing, and gym weights are all designed to give the user grip.

It has been shown that tactile friction can be reasonably modeled as a summation of friction from adhesion and deformation (Adams et al., 2007), adhesion being the dominant mechanism (Adams et al., 2007; Tomlinson et al., 2009). Experiments have shown that coefficient of friction decreases as surface roughness is increased from a nominally smooth surface (Skedung et al., 2010; Derler et al., 2009). This has been attributed to a reduction in real contact area reducing the amount of adhesion between the two surfaces. However, once a certain roughness is achieved the friction increases sharply. Tomlinson et al. (Tomlinson et al., 2011) experimented with triangular ridged surfaces of varying sizes and showed that when the surface roughness was increased to a certain threshold, an increase in friction was seen. This is attributed to an increase of the deformation component of friction by viscoelastic hysteresis and interlocking. They also noted that when groove depth was shallow, adhesion still occurred because the penetration of the finger into the grooves had reached the bottom of the groove channels. Darden et al. (Darden and Schwartz, 2013) hypothesized about the same phenomenon when testing the effect of sliding direction on friction against parallel-ridge textures. They investigated the sliding of a spherical neoprene probe parallel to and perpendicular to the orientation of ridges on a simple

* Corresponding author.
E-mail address: cris1@iastate.edu (C.J. Schwartz).

http://dx.doi.org/10.1016/j.ijsolstr.2016.05.013
0020-7683/

parallel-ridge textured surface. When the textural ridges were below a certain height, the coefficient of friction did not exhibit a change with sliding orientation, whereas ridges above this height showed a marked sliding orientation effect. Taylor and Lederman showed that the penetration of the finger into the groove is also an important factor in perception of roughness and developed a model to predict perceived surface roughness of parallel ridged surfaces as a function of penetration, groove width, and finger force (Taylor and Lederman, 1975). Zhang et al. further investigated such ridged surfaces and confirmed that the direction of sliding has a profound effect on the mechanisms of friction, which suggests that penetration of the soft fingertip into the intra-groove voids may contribute both to additional contact area as well as collision with ridge edges (Zhang, 2015). Correlations have been found between perceived roughness and friction (Chen et al., 2009; Bergmann Tiest, 2010; Smith et al., 2002). Numerous studies have also shown an increase in perceived roughness as groove width increases (Smith et al., 2002; Lederman, 1981; Kawasoe et al., 2008) which plays a crucial role in the amount of penetration that occurs.

The mechanics at the finger-on-texture interface are very complex, however, finite element analysis (FEA) has been utilized to model the interaction between fingers and surfaces to account for the complexities of the interaction and to analyze the stresses produced within the finger. Xydas et al. (2016) utilized FEA to determine the effect of adhesive friction on contact area of a finger on a flat surface using experimental friction measurements. Maeno et al. (Maeno et al., 1998) utilized FEA to model the internal stresses within the finger during movement along a flat surface taking into account the epidermal ridges, papillae, and bone and found that tactile receptors are appropriately located in areas of maximum von Mises stress produced by the shearing of the epidermal ridges. Shao et al. (Shao et al., 2010) conducted a similar FEA study analyzing the effect of epidermal ridges on the oscillation of friction force and location of maximum von Mises stress when the finger interacts with a textured surface.

Because of the observed impact on friction coefficient of fingertip penetration into textural features, this investigation sought to better understand the mechanics of penetration of the finger into textural grooves, because of its importance in designing textures with desired levels of friction or perceived roughness. Accurately predicting the amount of penetration into textural grooves would help to predict the likelihood of micro-adhesion at the bottom of the groove channels, provide insight in the perception of surface roughness, and possibly provide insight to predicting the amount of friction due to deformation. There currently lacks an analytical solution, such as those presented by Hertz for the contact distance of a cylinder against a rigid plane, for the penetration of a cylinder as it is compressed against a rigid grooved surface.

The objective of this study was to develop a model to predict the amount of penetration of a soft cylindrical body into a rigid parallel rectangular grooved surface to simulate finger-on-texture contact. The parameters considered in this interaction included the widths of the surface grooves and ridges as well as the radius of the cylinder, elastic modulus, and applied pressure. Parameters of similitude were non-dimensionalized with one another as input variables to make the model applicable to both the micro and macro scale. An analytical mechanical approach was taken as a basis of the relationship between applied load and penetration. The model was developed by the regression of the penetration results of numerous FE simulations which varied the groove width in a particular range of interest applicable to the surface textures used in experiments of Darden et al. (Darden and Schwartz, 2013). The effect of multiple grooves on penetration was also analyzed in order to better model realistic textures.

2. Methods

The methodology of this investigation was to develop a model to predict penetration of an elastomeric cylindrical body into rectangular rigid grooves, based on textural geometry parameters and elastomer stiffness. To attain this goal, an FE model of both the cylinder and texture were developed and studied. FE results were compared to data collected from an experimental apparatus in order to validate the FE model, and finally the effects of additional grooves were studied using the model. The dimensionless parameters of the model were determined by dimensional analysis via Buckingham Pi theory. This approach allows for the development of a scale-invariant conceptual model of a system using dimensionless terms in order to evaluate results when experiments are run at different size and/or time scales compared to the original phenomenon. The approach is commonly used in experimental fluid mechanics and heat transfer, but also provided value in this work. The structure of the proposed non-dimensional model was determined both by an analytical technique and using a least squares regression to several data resulting from numerous FEA simulations.

2.1. Texture parameters and similitude approach

The modeled textures were two-dimensional parallel ridges with rectangular cross section. The space between the ridges (referred to as 'grooves') is referred to as '*b*', while ridge is referred to as '*a*'. The cylinder which was loaded into the textured is defined by its radius, *R*, elastic modulus, E, and Poisson ratio, *v*. A load was applied to a rigid horizontal plate which rested above the cylinder. The applied load per unit length, divided by the cylinders diameter is denoted by '*p*'. The output parameter of interest is the total penetration, δ_{tot}, of the cylinder into the central groove. The total penetration is a combination the initial penetration, δ_i, as the cylinder rests atop the central groove without any external loading, and the forced penetration, δ_f, which is the penetration caused from the applied loading. The initial penetration (based solely on cylinder radius and groove width) was calculated using trigonometry of a circle of radius, *R*, resting atop two ridges with a fillet radius, *r*, spaced a distance, *b*. This initial penetration, δ_i, can be calculated by

$$\delta_i = R + r - \sqrt{(R+r)^2 - \left(\frac{b}{2} + r\right)^2} \tag{1}$$

While the fillet radius affects δ_i, for the purpose of this experiment, it is assumed to be small enough to have a negligible effect on δ_f. Fig. 1 shows both the uncompressed and compressed state of a cylinder interacting with a grooved surface. Dimensionless parameters of similitude were selected as input parameters for the model through the use of Buckingham Pi theory. From these parameters, there were two dimensions including length and force. This left the unique variables in each Π term to be δ_f, *p*, and *b*, respectively.

The use of dimensional analysis yielded the output dimensionless parameter involving penetration, δ_f/R, and the input parameters p/E and b/R which depend on load, geometry and material properties. The contribution from each input parameter was determined by the analytical and FEA methods in the following sections.

2.2. Mechanics basis for finite element approach

In an attempt to determine an analogous phenomenon that possessed a closed-form analytical solution to serve as the basis of a regression model, the penetration of the cylinder into the

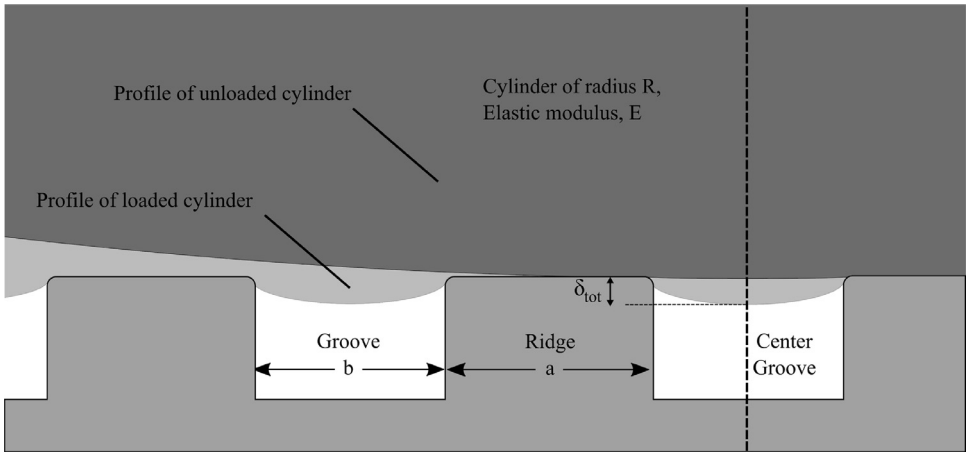

Fig. 1. Depiction of the parameters which govern the penetration of a soft cylinder into a rigid grooved surface.

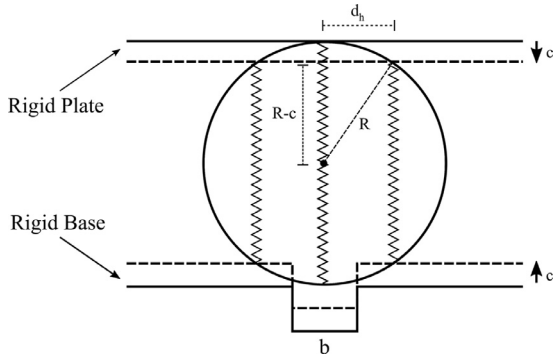

Fig. 2. The compressive force of a cylinder can be modeled as a summation of springs. Five springs are displayed (two are infinitely small at the sides of the cylinder). Contact distance is calculated using Pythagorean theorem.

grooved rigid body was modeled by the compression of parallel infinitesimal springs that make up the body of the cylinder between a rigid plate and a single rigid groove. Although this one-dimensional simplification ignored the transverse behavior due to shear and Poisson effects, it provided a useful overarching conceptual framework. Fig. 2 illustrates this parallel-spring model. The total compression of the cylinder, c, is equal to the distance the center spring penetrates into the groove. The compression of an individual spring, c_s, is equal to the difference in length between the length of the spring, L_s, and the center spring, L_{cs}, subtracted from $2c$ or

$$c_s = 2c - (L_{cs} - L_s) \tag{2}$$

L_{cs} is equal to $2R$, and L_s was determined by geometry and the spring's horizontal distance from the center, x_s. Eq. (2) then becomes

$$c_s = 2c - \left(2R - 2\sqrt{R^2 - x_s^2}\right) \tag{3}$$

Assuming the same spring constant for each spring, the resulting force for a given compression is a function of the summation of the compressions of all springs in contact with the rigid plates and normalized by the number of finite springs. This can be seen by

$$force \sim \sum_{s=s_b}^{s=s_d} \frac{2c - 2R + 2\sqrt{R^2 - x_s^2}}{\#Springs} \tag{4}$$

where s_b is the first spring in contact with the base plate located at half the groove width from the center of the circle and s_d is the last spring in contact with both the pressing plate and base. Each spring's position, x_s, was determined by the even distribution of springs along the diameter of the circle. The spring was considered to be in contact if the absolute value of its position is within the half-contact distance, d_h, which is determined by geometry and c to be

$$d_h = \sqrt{2Rc - c^2} \tag{5}$$

This approach is shown in the figure, but with only three springs displayed for simplicity. Solutions to (4) were determined by using a computational algorithm, and a least squares regression was used to determine the direct relationship between the compression of a cylinder and the resulting force.

2.3. Finite element model

A two-dimensional FEA model (Abaqus/CAE v6.12) was constructed to investigate the relationship between the applied load on a cylindrical body resting on a single grooved rigid body and the resultant forced penetration, δ_f, into the groove as seen by Fig. 3. An eight-node biquadratic plain strain quadrilateral element was used with full integration. Plain strain elements were chosen because deformation outside of the plane was assumed to be negligible for both tactile studies and the experimental apparatus consisting of a long polyurethane cylinder.

The cylinder was modeled to be linearly elastic and inertial effects were neglected. The Poisson ratio, ν, was set to 0.49 to model nearly incompressible behavior. The ratio of groove width to cylinder radius (b/R) was varied from 0.01 to 0.1 in increments of 0.01. The ratio of load per unit length to elastic modulus (p/E) was varied from 0 to 0.03 in a total of 1000 increments or until excessive deformation occurred at which point model solution iteration could not proceed. The selected b/R range was of particular interest because it incorporated the range of groove sizes used in tactile friction experiments used by Darden et al. Moreover, this particular range targeted the hypothesized threshold of the human ability to discriminate gaps as indicated by Johnson et al. (Johnson and Phillips, 1981) assuming the finger is modeled as a cylinder with a diameter equal to the short axis of the finger as measured by Maeno et al. (Maeno et al., 1998).

A static implicit step was used in the FE approach with a history output tracking the location of the center node of the bottom surface of the cylinder. This history output enforced a penetration calculation at 1000 intervals of the total load. A constraint was placed on the vertical centerline of the circle to prevent movement in the x direction which both kept the object stable and

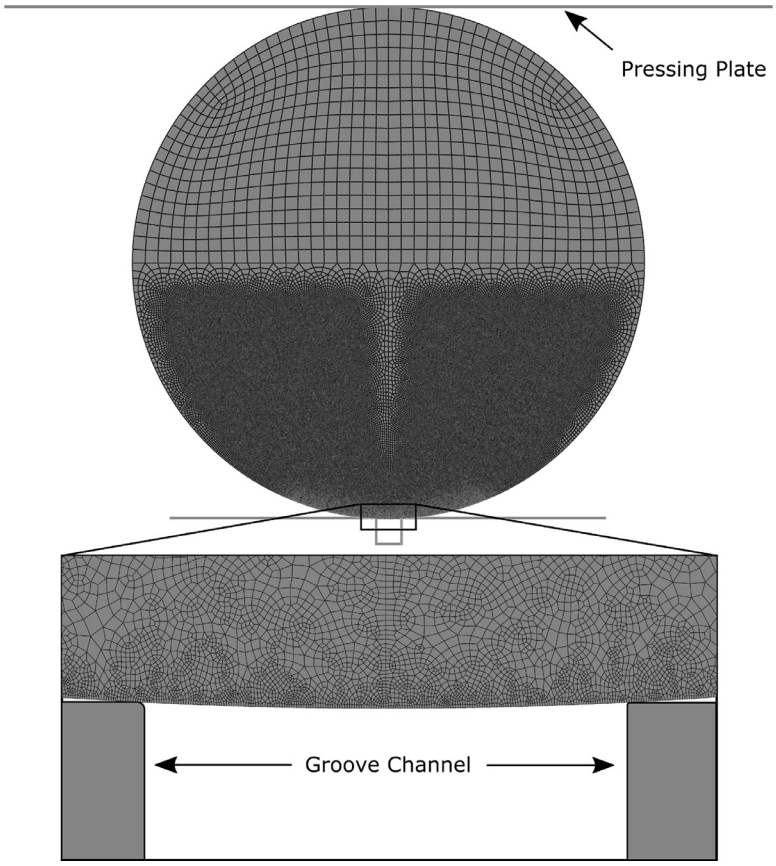

Fig. 3. Overview of assembly with detail of refined mesh near groove with b/R equal to 0.1.

allowed for accurate penetration calculations. The adhesive coefficient of friction between the interacting surfaces was set to 0 to focus solely on the effect of geometry and load. After the FE model was physically validated (see below), simulations were run with additional grooves to determine their effect on penetration. These simulations were run on all combinations of 3, 5, and 7 grooves with b/R values of 0.01, 0.02, 0.03 and a/R values of 0.012, 0.022, and 0.032.

2.4. Physical validation of numerical model

An experimental apparatus was built in order to collect penetration data to validate the FE model results. Because the FEA model used dimensionless parameters of similitude, the physical apparatus was able to be constructed on the macro scale, allowing the penetration to be easily measured. This change in scale was the impetus for the adoption of the non-dimensional approach described above. The apparatus consisted of a steel plate which was mounted on four rods with linear bearings which allowed for displacement in the vertical direction as shown by Fig. 4, and three different polyurethane cylinders with varying elastic moduli. The polyurethane cylinder rested atop two aluminum blocks which were displaced a desired distance and fixed in order to model two ridges separated by a groove. The area on the top of the pressing plate allowed for the use of calibration weights to be stacked for load application. Once loaded, a digital microscope (AM2111 Dino-Lite Basic) was used to acquire images of the front face of the polyurethane cylinder. These images were then analyzed using image analysis software (ImageJ 1.48) to determine total penetration into the groove.

The elastic modulus was determined for each of the polyurethane cylinders using an analytical solution which describes the compression of a cylinder onto a plane (Puttock and Thwaite, 1969) given by

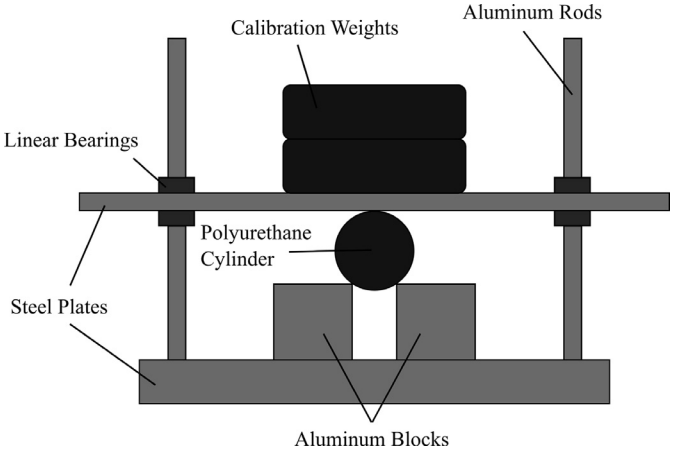

Fig. 4. The apparatus consists of a steel plate mounted on four rods and a polyurethane cylinder which rests on two aluminum bars. Load was applied by setting calibration weights on the top steel plate which moves freely in the vertical direction.

$$\alpha = \bar{P} \cdot (V_1 + V_2) \cdot \left[1 + \ln \left\{ \frac{8a^2}{(V_1 + V_2) \cdot \bar{P} \cdot D} \right\} \right] \tag{6}$$

$$V = \frac{1 - \nu^2}{\pi E} \tag{7}$$

where 2α is the total compressed distance when loaded between two planes, $\bar{P}$ is the load per unit length, 2a is the length of

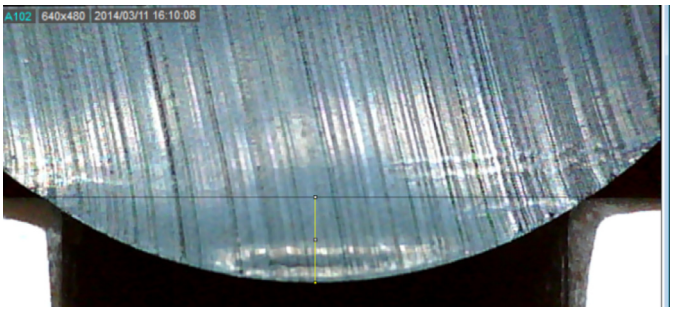

Fig. 5. Cylinder 3 loaded with 7 N on gap size $b/R = 1.0$ as measured by ImageJ.

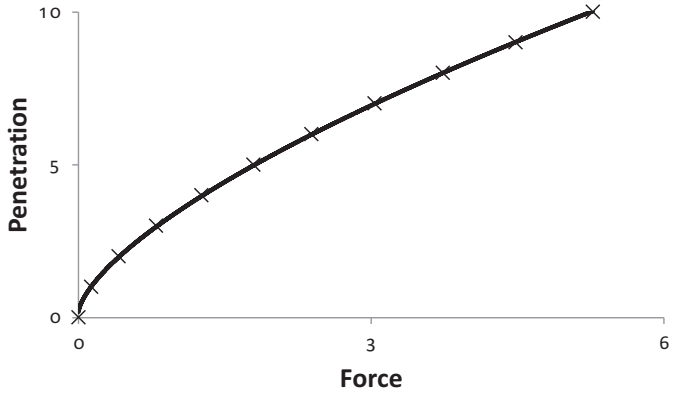

Fig. 6. The algorithm which implements (4) was tested with R = 100 and b/R = 0.03 and the results are denoted by 'x'. The regression shown by (8) represents this data with high accuracy ($R^2 = 1$).

the cylinder, D is the diameter, and V is a material constant. Because the steel plates have a much higher elastic modulus than the polyurethane, V_2 was assumed to have a negligible effect and is ignored. Compression tests were conducted on each of the polyurethane cylinders using the experimental apparatus without the blocks present. An image was taken of each cylinder before compression to calibrate the ImageJ software followed by an image of each cylinder compressed with a known load. The elastic moduli for the three polyurethane cylinders were calculated to be 1.1 ksi, 2.0 ksi, and 2.7 ksi, each having a Poisson ratio of 0.49. Fig. 5 shows the penetration being measured of a sample in ImageJ. The images were then calibrated using the known distance between the two aluminum blocks. Because each of the three cylinders had some warping, the penetration was measured for each trial four times at rotational angles of 0°, 90°, 180°, 270°. The order of data collection was randomized to address stochastic variation and potential anisotropy in the cylinder behavior. The standard error of the measurement was also determined to estimate the overall experimental uncertainty.

3. Results and discussion

The computational algorithm developed for the infinitesimal spring concept was implemented with several combinations of R and b. Using a least squares regression on the results from the algorithm, the relationship between load, P, and penetration, δ, was determined to be

$$\delta = m \cdot P^{2/3} + n \tag{8}$$

where m and n are fit parameters which depend on cylinder radius and groove width. The penetration data for each combination of R and b resulted in a very high correlation ($R^2 > 0.99$) to (8).

When examining the penetration data from the FE simulations, the relationship between load and penetration was isolated by examining each b/R case individually. By conducting a least squares regression of each b/R case, a power relationship was determined between loading and penetration with the best fit ($R^2 = 1$) case resulting with an exponent varying between 0.6 and 0.7. Because the parallel-infinitesimal spring concept resulted in an exponent of 2/3, the following relationship was applied to each b/R case from the FE simulations

$$\delta_f/R = K \cdot (p/E)^{2/3} \tag{9}$$

This resulted in a correlation coefficient of over 0.99 for each b/R case. The parameter K varied linearly between groove sizes. The effect of b/R on forced penetration was isolated by using a constant load to cause the cylinder to penetrate into grooves of varying b/R values. Fig. 7 shows that the forced penetration is linearly dependent on b/R. Incorporating this linear relationship into (9) results in

$$\delta_f/R = K \cdot b/R \cdot (p/E)^{2/3} \tag{10}$$

The value of K was found to be 1.282 using a least squares regression resulting in the following model for the overall cylinder penetration into the central groove:

$$\delta_{tot}/R = 1.282 \cdot b/R \cdot (p/E)^{2/3} + \delta_i/R \tag{11}$$

Fig. 8 shows the results from the model overlaid with the data collected from each FE simulation and indicates a strong correlation ($R^2 = 0.992$).

Fig. 9 shows the penetration results of the physical validation experiment using a b/R value of 0.5 compared with the predictions

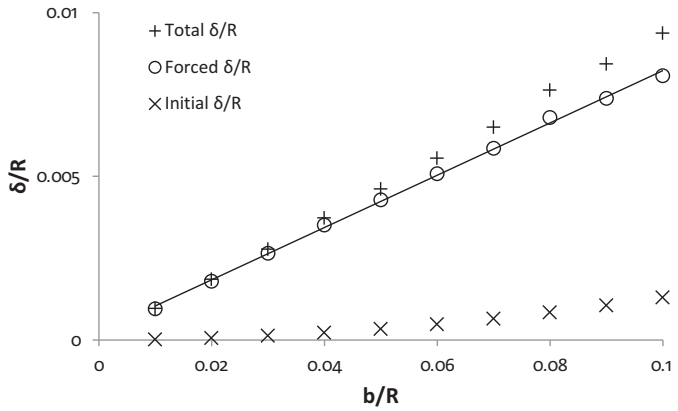

Fig. 7. The total penetration predicted by the numerical model with respect to groove size when p/E is kept constant at 0.017 shows a highly linear relationship between groove size and penetration due to load.

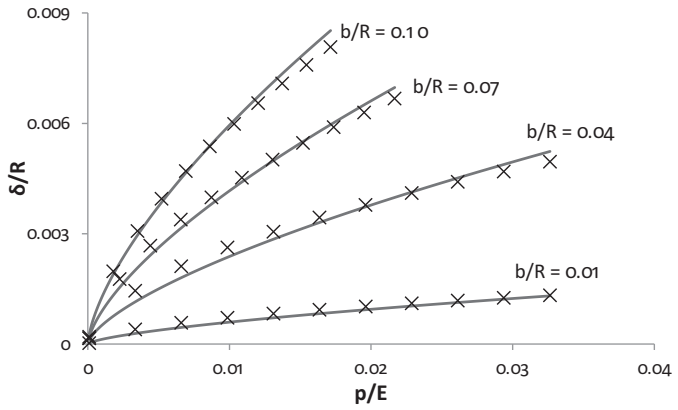

Fig. 8. Penetration as a function of p/E and b/R. Data from individual simulations are represented by data points and overlaid with results from the model.

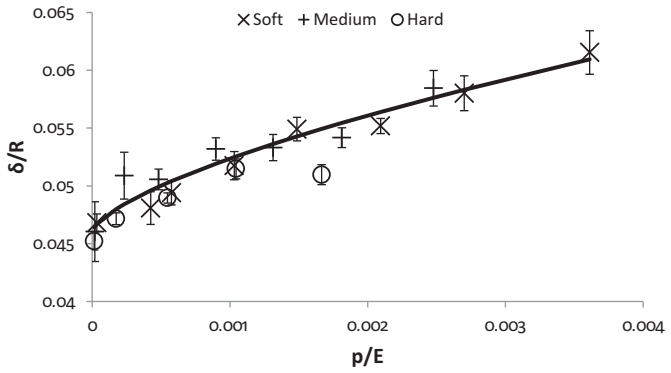

Fig. 9. Model prediction for normalized penetration compared with experimental penetration results of three polyurethane samples of varying elastic modulus into a gap of $b/R = 0.5$.

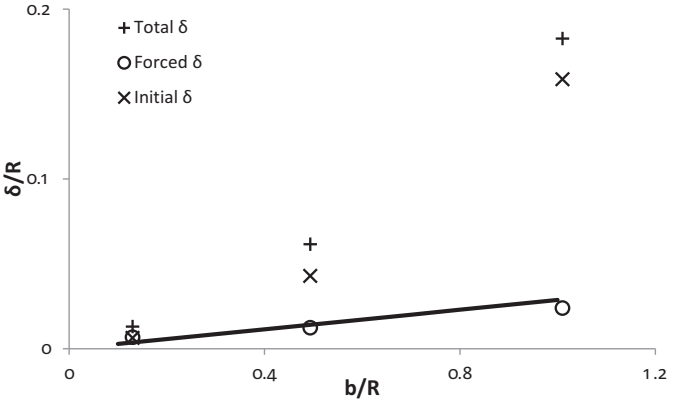

Fig. 10. The experimental penetration as a function of b/R with a constant p/E. The total penetration of the experiment is dependent mostly the initial penetration due to the relatively high values elastic modulus.

from the FE penetration model as a function of load. When loading is kept constant, the penetration can be seen as a function of b/R as seen by Fig. 10.

The correlation factor calculated between the model and the experimental data for b/R values of 0.12, 0.5, and 1.0 are 0.83, 0.91, and 0.91, respectively, showing that the model predicted penetration with high accuracy. The simulations with the smallest groove-to-radius ratio ($b/R = 0.12$) was likely the least accurate because of a higher sensitively to both the tolerance of parallelism between the two blocks and the slight warping of the polyurethane cylinders. Another important point to consider is the relatively high elastic modulus of the polyurethanes. This caused the forced penetration to be relatively small compared to the extent of penetration seen in the FE simulations. Fig. 10 clearly shows that the total penetration of the experiment is dominated by the initial penetration. Future experiments with increased p/E values would be useful in validating the model further so that there would be a greater amount of forced penetration.

Geometrically, the initial penetration is dependent on the groove width to the power of 2 which led to the hypothesis that forced penetration would follow a similar trend. However, the forced penetration increased linearly with respect to groove width when load was kept constant. This finding led to the model developed in Eq. (11). In order to address the difficulties in modeling sharp corners with finite element methods, the model incorporated a small radius of curvature of the ridge edges (a ratio of ridge-edge radius of curvature to the radius of the deformable body of 0.001).

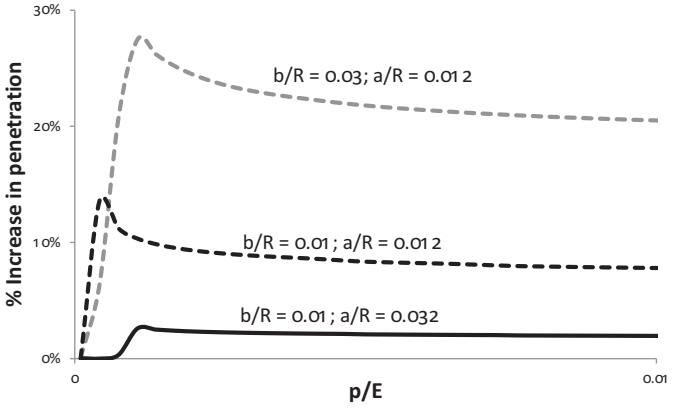

Fig. 11. When the number of grooves is increased from 1 to 3, the increase in penetration is more significant for larger b/R ratios and smaller a/R ratios. The increase in penetration grows significantly as the cylinder penetrates into the adjacent grooves but levels off after contacting the outer edge of the adjacent grooves.

It was assumed that the corners' contribution to forced penetration was negligible. The change in initial penetration from varying radii of curvature of the groove edges was accounted for by Eq. (1).

Additional simulations were conducted to determine the effect of additional grooves on the penetration into the center groove. Thus, a new parameter representing the width of a ridge was introduced into the model (denoted by a) and normalized to the cylinder radius by a/R. In these simulations, b/R ratios of 0.01, 0.02, 0.03 were chosen as well as a/R ratios of 0.012, 0.022, and 0.032. These parameters were used with simulations of 3, 5, and 7 grooves. The presence of additional grooves resulted in an increase in penetration into the center groove. The increase in grooves had a greater impact on penetration with larger b/R values and lower a/R values as seen by Fig. 11. While the shift from 1 groove to 3 grooves showed a significant impact on penetration, the increase to 5 and 7 grooves resulted in a negligible increase in penetration for the given loading range. Thus, the amount of penetration into a surface with a large number of grooves can be accurately predicted by only modeling the grooved surface as having 3 grooves. It is hypothesized that increasing the groove count above 3 may have an impact on penetration into the center groove for higher loads or a higher ratio of b/R to a/R.

As previously mentioned, Darden et al. (Darden and Schwartz, 2013) investigated the sliding of a neoprene sphere across parallel ridged surfaces of varying grooved width, ridge width, and ridge height. Although the model presented in this paper assumed a cylindrical shape for the deformable body, it provides insight to their results by predicting whether the neoprene sphere is in contact with the bottom of the grooves. When the groove and edge widths were normalized with the radius of the neoprene ball, the b/R values varied between 0.007 and 0.05 while the a/R values varied between 0.012 and 0.04. In their experiment, a force of 7 N was applied to the neoprene ball. The p/E value used in their experiment was found by doing a similar compression tests on the neoprene ball and utilizing ImageJ to find the compression and therefore an elastic modulus. The compressive stiffness of the neoprene ball was found to be 1.4 ksi which results in a p/E value of 0.003.

Applying the model derived in this paper, which only takes into consideration one groove, it was found that penetration would be between 30% and 45% of the ridge heights. However, the effect of additional grooves in this paper for a b/R value of 0.03 led to a fourfold increase in penetration at p/E value of 0.003. This clearly suggests that with shorter ridge heights, the directionality

of sliding friction is reduced because the penetration is sufficient to contact the bottom surface of the groove, providing additional contact area for adhesive friction.

This model is also insightful when compared to the findings of Tomlinson et al., whose work showed that at shallow groove depths adhesion was still the dominant mechanism, but at deep depths, the interlocking term was much more pronounced. The model can be used to bridge the gap of determining at what depth the friction mechanisms would change so as to more accurately model tactile friction. In addition, Taylor and Lederman (Taylor and Lederman, 1975) showed that penetration was of importance to tactile perception. Having an accurate prediction of penetration may be an indicator of the perception of roughness.

Future work with computational models similar to that used in this study may involve sliding the deformable cylinder over the parallel grooves with a compressive load as opposed to the current static compression. Utilizing a sliding step with frictionless surfaces, the frictional force due to deformation and penetration could be investigated computationally and correlated with groove size and compressive load. The experiment could also be improved in the future by using deformable cylinders of a very fine degree of warping and also ensuring a very small tolerance of parallelism of the groove edges in addition to incorporating sliding motion.

4. Conclusions

- The finite element computational model results suggest that groove penetration can be very well modeled by a simple non-dimensional relationship that incorporates the ratios of groove width to cylinder radius, applied load per unit area to elastic modulus, and initial geometry-based unloaded penetration. This empirical relationship allows for penetration to be incorporated into skin friction models based on interlocking with textural features.
- The model showed a good correlation with the experimental data obtained from polyurethane cylinders loaded onto a single groove. Error was expected due to the slight warping of the cylinders, parallelism of the aluminum blocks, precision of the image analysis method, and the relatively low amount of total penetration due to forced penetration.
- Elastomer penetration into a center groove is increased by the presence of additional parallel groves, as would be encountered in a uniform parallel-ridged texture. An increase in number of grooves beyond three had a minimal effect for the elastic modulus, load range, groove and ridge widths investigated here.

References

Adams, M.J., Briscoe, B.J., Johnson, S.A., 2007. Friction and lubrication of human skin. Tribol. Lett. 26 (3), 239–253.
Barnes, C.J., et al., 2004. Surface finish and touch—a case study in a new human factors tribology. Wear 257 (7), 740–750.
Bergmann Tiest, W.M., 2010. Tactual perception of material properties. Vision Res. 50 (24), 2775–2782.
Chen, X., et al., 2009. Materials' tactile testing and characterisation for consumer products' affective packaging design. Mater. Des. 30 (10), 4299–4310.
Childs, T.H.C., Henson, B., 2007. Human tactile perception of screen-printed surfaces: self-report and contact mechanics experiments. Proc. Inst. Mech. Eng. Part J J. Eng. Tribol. 221 (3), 427–441.
Darden, M.A., Schwartz, C.J., 2013. Investigation of friction mechanisms during the sliding of elastomers against hard parallel-ridge textures. Tribol. Int. 63, 2–7.
Derler, S., et al., 2009. Influence of surface microstructure on the sliding friction of plantar skin against hard substrates. Wear 267 (5), 1281–1288.
Johnson, K.O., Phillips, J.R., 1981. Tactile spatial resolution. I. Two-point discrimination, gap detection, grating resolution, and letter recognition. J. Neurophysiol. 46 (6), 1177–1192.
Kawasoe, T., Kakizawa, M., Shimizu, H., 2008. Tribology in the hair surface and tactile perception. Tribol. Online 3 (2), 127–130.
Lederman, S.J., 1981. The perception of surface roughness by active and passive touch. Bull. Psychonom. Soc. 18 (5), 253–255.
Maeno, T., Kobayashi, K., Yamazaki, N., 1998. Relationship between the structure of human finger tissue and the location of tactile receptors. JSME Int. J. Ser. C 41 (1), 94–100.
Puttock, M.J., Thwaite, E.G., 1969. Elastic Compression of Spheres and Cylinders at Point and Line Contact. Commonwealth Scientific and Industrial Research Organization, Melbourne, VIC, Australia.
Shao, F., et al., 2010. Finite element simulations of static and sliding contact between a human fingertip and textured surfaces. Tribol. Int. 43 (12), 2308–2316.
Skedung, L., et al., 2010. Finger friction measurements on coated and uncoated printing papers. Tribol. Lett. 37 (2), 389–399.
Smith, A.M., et al., 2002. Role of friction and tangential force variation in the subjective scaling of tactile roughness. Exp. Brain. Res. 144 (2), 211–223.
Taylor, M.M., Lederman, S.J., 1975. Tactile roughness of grooved surfaces: a model and the effect of friction. Percept. Psychophys. 17 (1), 23–36.
Tomlinson, S.E., et al., 2011. Human finger contact with small, triangular ridged surfaces. Wear 271 (9), 2346–2353.
Tomlinson, S.E., Lewis, R., Carré, M.J., 2009. The effect of normal force and roughness on friction in human finger contact. Wear 267 (5), 1311–1318.
Xydas, N., Bhagavat, M., Kao, I., 2000. Study of soft-finger contact mechanics using finite elements analysis and experiments. In: Proceedings of the IEEE International Conference on Robotics and Automation, ICRA'00, vol. 3. IEEE, pp. 2179–2184.
Zhang, S., 2015. The role of the sliding direction against a grooved channel texture on tool steel: an experimental study on tactile friction. Int. J. Solids Struct. 53–61 56–57.